RESEARCH ARTICLE

Bandwidth Dependence of the Propagation Channel in Circular Metallic BAN Environments

MANUEL M. FERREIRA[1,2], **(Member, IEEE), FILIPE D. CARDOSO**[1,2], **(Member, IEEE),**
SŁAWOMIR J. AMBROZIAK[3,4], **(Senior Member, IEEE),**
AND LUIS M. CORREIA[5], **(Senior Member, IEEE)**

[1]ESTSetúbal, Instituto Politécnico de Setúbal, 2914-508 Setúbal, Portugal
[2]INESC-ID, 1000-029 Lisbon, Portugal
[3]Faculty of Electronics, Telecommunications and Informatics, Gdańsk University of Technology, 80-233 Gdańsk, Poland
[4]Digital Technologies Center, Gdańsk University of Technology, 80-233 Gdańsk, Poland
[5]IST/INESC-ID, University of Lisbon, 1049-001 Lisbon, Portugal

Corresponding author: Filipe D. Cardoso (filipe.cardoso@estsetubal.ips.pt)

ABSTRACT In this paper, the bandwidth dependence of the propagation channel for Body Area Networks (BANs) in circular metallic environments is addressed and models are proposed to evaluate the appropriate short-term fading margins that should be considered as a function of the system bandwidth. The deployment of BANs in metallic indoor environments, such as ships, factories, warehouses and other similar environments, involves additional challenges compared to other indoor environments due to the specific propagation effects in this type of environments (i.e., with strong reflections). No studies of this kind and for this type of environment can be found in literature, giving the motivation for this work. Bandwidth dependent values of delay spread are also presented and discussed. It is observed that for a system bandwidth up to 100 MHz the fading depth is composed of three main stages, with the transitions between these stages being associated with the system ability to discriminate arriving rays at the receiver. Average values of fading depth are 16.4, 13.2 and 11.0 dB for stages 1, 2 and 3, respectively, the difference between consecutive stages ranging between 2.2 to 3.2 dB. For a system bandwidth larger than 100 MHz, the fading depth decreases with an increasing system bandwidth, with an average decay rate close to 3 dB per 100 MHz bandwidth, being about 2 dB for system bandwidths above 400 MHz.

INDEX TERMS Body area networks, metallic structures, propagation channel, fading-depth, short-term fading margin, bandwidth dependence.

I. INTRODUCTION

With the development of Body Area Networks (BANs) the use of this kind of networks in unusual environments, such as ships, factories, warehouses, and other environments where walls and ceilings are usually a metallic structure, becomes of interest. Several studies address channel characterization in this kind of environments, [1], [2], [3], [4], [5], but none address either the particular aspects of BANs or the specific problem of metallic structures.

The associate editor coordinating the review of this manuscript and approving it for publication was Faissal El Bouanani.

There is limited research on BAN propagation channels in metallic environments. In [6] and [7] propagation inside circular metallic structures is addressed and a propagation channel simulator is proposed and assessed with measurements at 2.45 GHz. In these works, a fading analysis is performed, fast fading statistical distribution parameters are derived and the temporal characteristics of the propagation channel in circular metallic environments are modelled. Still, no analysis on the propagation channel dependence on the system bandwidth is addressed, therefore creating a gap that really needs to be fulfilled, since existing systems have different, or variable, system bandwidths. From the cellular

planning viewpoint, it is important to estimate possible network configurations and equipment required to achieve the required coverage with the desired capacity and quality of service.

Among many other parameters, long- and short-term fading margins are required to perform an appropriate link budget evaluation. Usually, a Log-Normal Distribution is used for modelling long-term fading effects, while short-term ones are usually derived from Rayleigh or Rice Distributions, i.e., system bandwidth and environment characteristics are not usually accounted for. However, the short-term fading margin depends on the environment being considered and on the system bandwidth, thus, results obtained while not considering this influence can originate large cell range estimation errors, leading to smaller cells, increased network deployment costs, or high transmitted powers, hence, more interference and lower link quality. Therefore, the use of appropriate fading margins enables a more accurate cell range prediction and a better radio network planning.

The problem of the propagation channel dependence on system bandwidth, hence, of the fading margins that need to be considered, was already addressed in the past [8], [9], [10], [11], [12]. Still, as far as the authors are aware of, no such studies exist for BANs in indoor circular metallic environments.

In this paper, the bandwidth dependent characteristics of the propagation channel for BANs in indoor circular metallic environments is addressed and a bandwidth dependent approach for the fading depth evaluation is proposed, allowing to evaluate the appropriate short-term fading margins. Additionally, bandwidth dependent values of delay spread are also presented and discussed. Hence, this work contributes for filling in the gap for proper approaches for evaluating channel parameters and fading depth in circular metallic BAN environments.

This paper is organized as follows. The channel model being used is described in Section II. In Section III, simulation results are presented, and the bandwidth dependence of the propagation channel is studied. In Section IV, a model for the evaluation of the fading margin required for radio network planning purposes is proposed and the obtained fading margins for different technologies are discussed. Conclusions are drawn in Section V.

II. BANDWIDTH DEPENDENT CHANNEL MODEL
A. INITIAL CONSIDERATIONS
The channel model being used in this work was proposed in [7], being applicable inside circular metallic structures. The model was assessed with measurements at 2.45 GHz in a circular room (a discotheque in a passenger ferry) with metallic walls and ceiling, in an 8 m radius; measurements were performed for typical situations occurring for BANs in off-body communications and on-body antenna placements. The model, and the corresponding simulator, provide a good accuracy by considering reflections only up to the 2nd order.
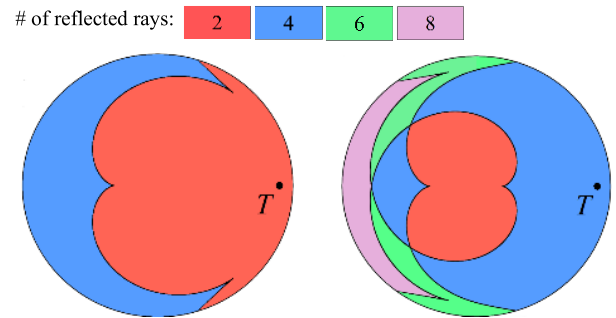

# of reflected rays: [2] [4] [6] [8]

FIGURE 1. Catacaustic regions for 1st (left) and 2nd (right) order reflections [7].

It must be noted that in the used model [7] Tx and Rx antennas are on a plane almost parallel to the floor, making it a 2D model. It is not expected that adding the third dimension (height) will change results significantly, since one has an environment with a significant number of reflections on walls and reflections on the floor and ceiling are less strong given that the radiation patterns of both antennas tend to have the maximum in the horizontal plane.

In a situation of off-body communications, between an on-body device and an Access Point, both can act as transmitter (Tx) and receiver (Rx). Usually, the Access Point is located on the wall or the ceiling, while the device can be located at any position inside the room. For the sake of simplicity, and without losing any generality in the analysis, one considers that the Access Point acts as the Tx while the device corresponds to the Rx, but the problem is a symmetric one, thus, the two positions are interchangeable.

For a fixed Tx position, the power at the Rx at any given location can be evaluated as the sum of the LoS component plus reflected ones. Assuming that the circular structure of radius R is composed of perfect conducting boundaries, given two points inside the circle, several reflections can be observed depending on the relative positioning of the pair (Tx, Rx).

Regions with a given number of reflections are defined as catacaustic zones. For illustration, Figure 1 shows the catacaustic regions for different Rx positions, when 1st and 2nd order reflections are considered, and the Tx is positioned in point T. It must be referred that the obtained catacaustic regions depend on the position of (Tx, Rx) in the circle, as detailed in [7].

B. DESCRIPTION OF CHANNEL MODEL
The model allows to properly describe propagation inside a circle with perfect conducting boundaries when up to M_{or} order reflections are considered and N_{rr} reflected rays are observed for the m-th reflection order. The Power Delay Profile (PDP) of the propagation channel $p(\tau)$ considering all n-th rays of the m-th reflection orders is [13]

$$p(\tau) = \sum_{m=1}^{M_{or}} \sum_{n=1}^{N_{rr}} k_A E_{mn}^2 \delta(\tau - \tau_{mn}) \tag{1}$$

where:

- k_A: constant depending on the antenna being used;
- E_{mn} : received electric field, such that

$$E_{mn}^2 = \frac{30\,P_t}{d_{mn}^2}\Gamma_{ref}^{2m} \tag{2}$$

- P_t: Tx power;
- Γ_{ref}^m : reflection coefficient;
- d_{mn} : path length;
- δ : Dirac's function;
- τ : absolute delay;
- τ_{mn} : delay relative to the Line-of-Sight (LoS) one.

As shown in [7], there is an analytical solution to the problem of finding the points where reflections take place on the circumference, but it involves the solutions of a quartic polynomial equation, and obtaining the actual solutions via analytical expressions is not a tractable problem, hence, numerical methods and a simulator being used to obtain solutions. Still, it is of value to understand the existing analytical solutions and to analyze some specific cases.

For the analysis of all possible positions of (Tx, Rx), given the circular geometry of the problem, it is enough to consider that the Tx is located on an axis at [0, R], while the Rx can occupy any position within the circle. Since one is looking for the delay profile, the quantity of interest for the evaluation of τ_{mn} is the path length difference between two arriving rays Δd_{mn},

$$\Delta d_{mn} = d_{mn} - d_{LoS} \tag{3}$$

where d_{LoS} is the LoS distance, so that

$$\tau_{mn} = \Delta d_{mn}/c \tag{4}$$

where c is the speed of light. In addition, when analyzing (2), one can take $\Gamma_{ref}^m = -1$ (due to the metallic walls), hence, the magnitude of the terms is basically defined by d_{mn}. Normalized distance parameters are defined, so that a nondimensional analysis can be conducted, for the path length, γ_{mn},

$$\gamma_{mn} = d_{mn}/R \tag{5}$$

and for the path length difference, β_{mn},

$$\beta_{mn} = \Delta d_{mn}/R \tag{6}$$

The problem of obtaining the distribution of the values that β_{mn} can take is not an analytically tractable one (as mentioned earlier), but some specific cases can be easily handled. One considers that the Tx can be at two "extreme" positions (the notation for the coordinates is the usual one, i.e., (x_T, y_T) for the Tx and (x_R, y_R) for the Rx):

- on the wall (i.e., on the circumference) at $(x_T = R, y_T = 0)$,
- at the center of the room (i.e., of the circumference) at $(x_T = 0, y_T = 0)$.

For each of these two cases, two other "extreme" positions can be taken for the Rx, on the x axis, i.e.: $(x_R = R, y_R = 0)$
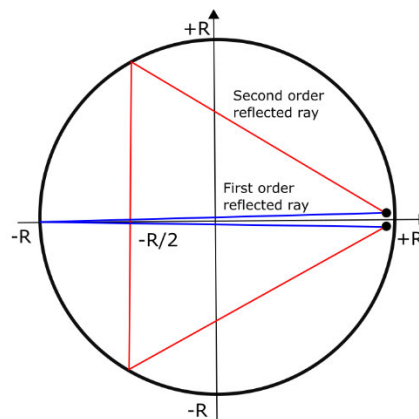

FIGURE 2. Examples of first and second order reflections.

and $(x_R = \text{-}R, y_R = 0)$ for the Tx on the wall, and $(x_R = 0, y_R = 0)$ and $(x_R = R, y_R = 0)$ for the Tx at the center. Due to the symmetry of the problem, the $(x_R = R, y_R = 0)$ position for the Tx at the center is equivalent to the $(x_R = 0, y_R = 0)$ one for the Tx on the wall, so one is covering all basic canonical positions that (Tx, Rx) can take. Figure 2 illustrates the case for (Tx, Rx) being on the wall (exact superposition is not taken, for a better understating of the geometric aspects), for 1$^\text{st}$ and 2$^\text{nd}$ order reflections.

In these specific cases, simple geometry can be used to obtain reflection points, from which it is easy to get Δd_{mn}. For this analysis, Tx and Rx are always considered to be on the x axis, hence, in what follows, one refers only to the x coordinates. Furthermore, one is assuming that both Tx and Rx are using omnidirectional antennas, so there is no spatial filtering of rays coming from the antennas.

The maximum values for the geometric parameters γ_{mn} and β_{mn}, γ_{max} and β_{max}, respectively, are given below, for a general value of M_{or}:

- $(x_T = R, x_R = R)$

$$N_{rr} = \begin{cases} 1, M_{or} = 1 \\ 2, M_{or} \neq 1 \end{cases} \tag{7}$$

$$d_{LoS} = 0 \tag{8}$$

$$\beta_{max} = \gamma_{max} = 2\,(M_{or} + 1)\sin\left(\frac{\pi}{M_{or} + 1}\right) \tag{9}$$

- $(x_T = R, x_R = \text{-}R)$

$$N_{rr} = 2 \tag{10}$$

$$d_{LoS} = 2R \tag{11}$$

$$\gamma_{max} = 2\,(M_{or} + 1)\sin\left(\frac{\pi}{2\,(M_{or} + 1)}\right) \tag{12}$$

$$\beta_{max} = \gamma_{max} - 2 \tag{13}$$

- $(x_T = 0, x_R = 0)$

$$N_{rr} = \infty \qquad (14)$$
$$d_{LoS} = 0 \qquad (15)$$
$$\beta_{max} = \gamma_{max} = 2M_{or} \qquad (16)$$

- $(x_T = 0, x_R = R)$

$$N_{rr} = 1 \qquad (17)$$
$$d_{LoS} = R \qquad (18)$$
$$\gamma_{max} = 2M_{or} + 1 \qquad (19)$$
$$\beta_{max} = \gamma_{max} - 1 (20) \qquad (20)$$

An analysis of these results reveals interesting features for γ_{max} and β_{max}, due to the very specific geometry of the environment, which should have implications on the decision where to install an Access Point (AP) in the room:

1) maxima occur at $(x_T = R, x_R = R)$ for $M_{or} =$1, 2, but for higher orders they do at $(x_T = 0, x_R = R)$;
2) for $M_{or} =$1, the maximum is $\beta_{max} = 4$, occurring for $(x_T = R, x_R = R)$;
3) for $M_{or} =$2, the maximum is $\beta_{max} = 3\sqrt{3} = 5.196$, occurring also for $(x_T = R, x_R = R)$;
4) $2M_{or}$ occurs for an infinite number of cases (due to the superposition of Tx/Rx at the center), and also it occurs twice for β_{max} (i.e., it is the same for $(x_T = 0, x_R = 0)$ and $(x_T = 0, x_R = R)$, hence, one should expect the occurrence of more reflections for this case;
5) for an increasing M_{or}, while the cases for $x_T = R$ lead to a saturation (at 2π and π, for γ_{max}), for $x_T = 0$ they lead to infinity, the behavior being an increasing monotonic one, despite of the sinusoidal functions.

Since τ_{mn} and E_{mn} depend on β_{mn} (the former is proportional to it and the latter is inversely proportional to its square), one can extract some consequences on the physical behavior of the reflected components of the signal:

- 1) and 5) imply that the location of the AP at the ceiling center or on the wall is not irrelevant, since the PDP will have a very different behavior, with implications on the quality of the signal;
- 4) implies that the placement of the AP on the wall will likely lead to lower values for the delay spread compared to locating it at ceiling center;
- 5) implies that for the AP on the wall, relative delays will not increase indefinitely, with decreasing magnitudes, for higher order reflections, rather showing an accumulation at specific values, while for the AP at the ceiling center, the usual behavior of increasing delays with decreasing magnitudes is observed;
- in a real environment, where walls and ceiling are not regular surfaces without objects, rather having quite a number of objects on it (e.g., lamps and frames, among many others), one can expect that low order rays tend to be the most important ones, higher order reflections tending to be obstructed by objects.
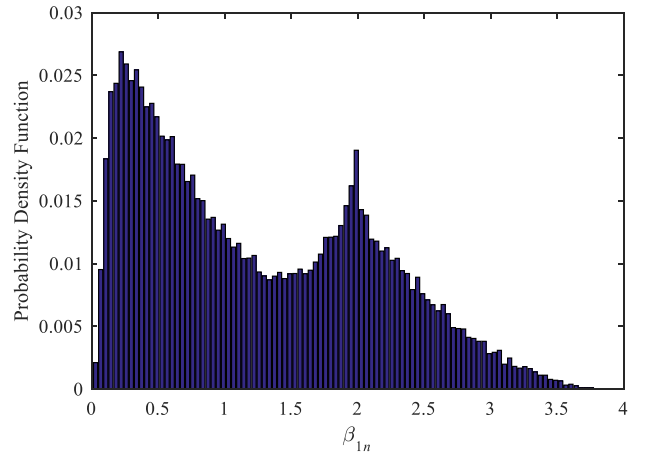


a) 1st order reflections.
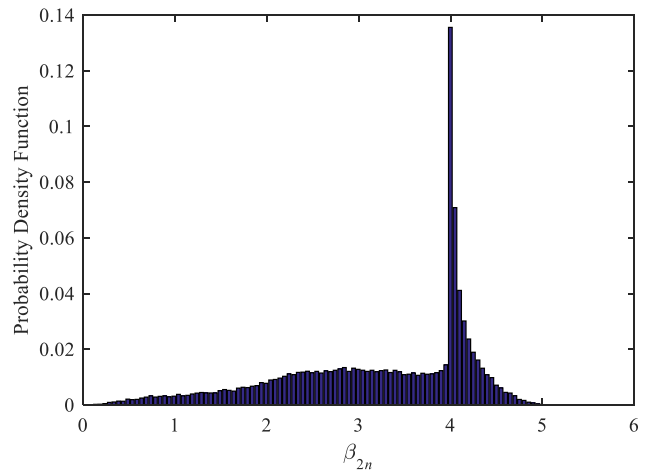
b) 2nd order reflections.

FIGURE 3. PDF of first and second order reflections vs. β_{mn}.

C. PRELIMINARY RESULTS ON CHANNEL PARAMETERS

Simulations were conducted for 25 000 (Tx, Rx) positions randomly distributed inside the circle when the Tx ranges in an axis at $[0, R]$, in order to obtain statistical distributions of 1st and 2nd order reflected rays, as a function of β_{mn}, Figure 3. The minimum distance to the wall for the Rx is 0.2 m to avoid algorithm convergence delays, hence, improving simulation time with no significant loss of physical meaning. It must be stressed that in a real situation the probability of the Rx to be positioned at a smaller distance from the wall is negligible.

Regarding the PDF of 1st order reflections, one can observe two maxima, at $\beta_{1n} = 0.22$ and $\beta_{1n} = 2$: the former is a consequence of the minimum distance to the wall taken for simulations and tends to zero when the minimum distance to the wall also tends to zero, being a consequence of the case when (Tx, Rx) are almost superimposed on the wall; the latter is coherent with observation 4). Furthermore, it is confirmed that β_{2n} has a maximum at 4, also confirming the theoretical analysis.

Since one has the values of β_{mn} and the power of each arriving ray, for each pair of locations, one can evaluate
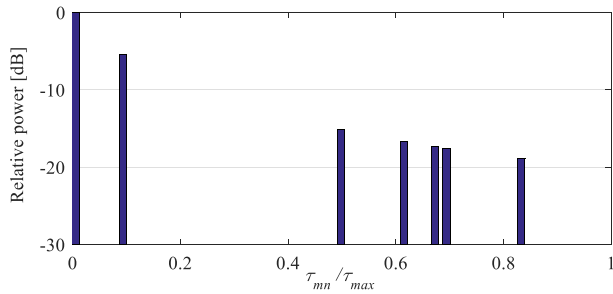
FIGURE 4. Example of a PDP for $M_{or} = 2$.
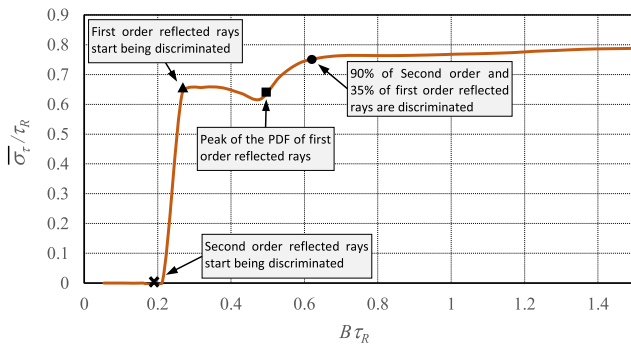
FIGURE 5. Average delay spread vs. B.

the PDP for each case, where the delay of each multipath component, τ_{mn}, is obtained from (4).

An example of a PDP for $M_{or} = 2$ is shown in Figure 4, which was obtained with the Tx and the Rx being positioned at $(0.53\,R, 0.0)$ and $(0.43\,R, 0.54\,R)$, were $\tau_{mn}/\tau_{max} = 1.0$ corresponds to an arriving ray with $\beta_{max} = 5.2$, i.e., the maximum value of β_{mn}. The obtained PDP is composed of 7 arriving rays corresponding to the LoS component plus 2 reflections of 1st order and 4 ones of 2nd order.

One is taking the PDP composed of all arriving rays, i.e., an infinite system bandwidth, B, is assumed; for any given value of B, the PDP can be evaluated by considering that all rays arriving within a time window of duration $1/B$ are not discriminated, i.e., they sum vectorially. By using this approach, one can obtain the PDP for any value of the system bandwidth.

For any given PDP and a value of B, the corresponding channel parameters can then be evaluated, e.g., the average delay spread, $\overline{\sigma_\tau}$, [13]. Similarly to the distances being normalized to the radius R, delays and frequencies are normalized to the delay associate with the radius, τ_R, i.e., the analysis is done on $B\tau_R$ and $\overline{\sigma_\tau}/\tau_R$ so that results are independent of R.

For illustration, taking the results of the previous simulations, Figure 5 shows the behavior of the average delay spread as a function of the system bandwidth. The meaning of the different breakpoints, B_{bp}, identified by the different symbols in Figure 5 is presented in Table 1. It must be noted that the minimum system bandwidth required to discriminate an

TABLE 1. Breakpoints.

Symbol	$B\tau_R$	B_{bp}	Meaning
✖	0.19	B_{D2nd}	2nd order reflections start being discriminated (β_{mn}=5.2)
▲	0.25	B_{D1st}	1st order reflections start being discriminated (β_{mn}=4.0)
■	0.50	B_{P1st}	1st order reflections peak of PDF (β_{mn}=2.0)
●	0.63	B_{C2nd}	2nd order reflections discriminated 90%, and 1st order ones discriminated 35% (β_{mn}=1.6)

arriving ray with a given value of Δd_{mn} is $c/\Delta d_{mn}$, hence,

$$B\tau_R = \frac{1}{\beta_{mn}} \quad (21)$$

As shown in Figure 5, the variation of $\overline{\sigma_\tau}/\tau_R$ as a function of $B\tau_R$ is composed of two main stages: the first one starts for $B\tau_R = B_{D1st}$ and the second one for $B\tau_R = B_{C2nd}$. For higher values of $B\tau_R$ one has $\overline{\sigma_\tau}/\tau_R$ practically constant, since most of the arriving waves are already discriminated.

III. ANALYSIS OF RESULTS
A. PARAMETERS USED IN THE ANALYSIS
Several parameters were considered for evaluating the propagation channel characteristics. The average delay spread, $\overline{\sigma_\tau}$, is evaluated as

$$\overline{\sigma_\tau} = \frac{\sum_{i=1}^{N_{PDP}} \left(\frac{\sum_{m=1}^{M_{or}} \sum_{n=1}^{N_{rr}} k_A E_{mni}^2 (\tau_{mni} - \overline{\tau_i})^2}{\sum_{m=1}^{M_{or}} \sum_{n=1}^{N_{rr}} k_A E_{mni}^2} \right)^{1/2}}{N_{PDP}} \quad (22)$$

where:

- $\overline{\tau_i}$: calculated as

$$\overline{\tau_i} = \frac{\sum_{m=1}^{M_{or}} \sum_{n=1}^{N_{rr}} k_A E_{mn}^2 \tau_{mn}}{\sum_{m=1}^{M_{or}} \sum_{n=1}^{N_{rr}} k_A E_{mn}^2} \quad (23)$$

- N_{PDP}: number of PDPs being considered,
- E_{mni}: E_{mn} for the i-th PDP;
- τ_{mni}: τ_{mn} for the i-th PDP;

Another key parameter for the characterization of a radio channel is the coherence bandwidth, since its comparison with system bandwidth is important for the design of systems in their operating environments, for which one can calculate its average, $\bar{B}_c$, [13], i.e. (for 90% correlation):

$$\bar{B}_c = \frac{1}{50\,\overline{\sigma_\tau}} \quad (24)$$

Additionally, the short-term fading depth, $D_{F1\%}$, is also considered, being evaluated as the difference in signal power corresponding to 1% and 50% of the cumulative distribution function (here noted as F_P) of the relative (referenced to its
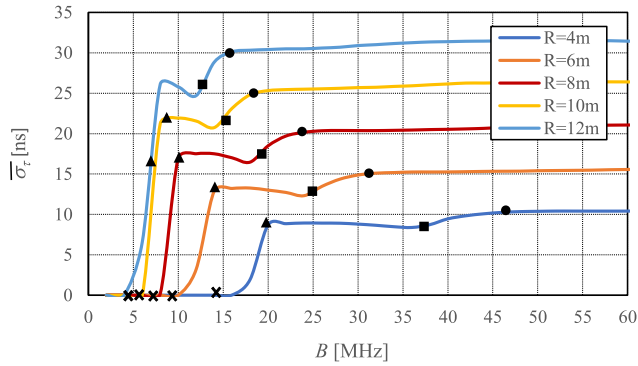
FIGURE 6. Average delay spread vs. B for various R.

TABLE 2. Average value and standard deviation of delay spread.

B [MHz]	$\overline{\sigma_\tau}$ [ns]					σ_{σ_τ} [ns]				
	R [m]					R [m]				
	4	6	8	10	12	4	6	8	10	12
10	0	0	16.9	21.9	25.8	0	0	10.7	13.2	15.6
20	8.7	13.0	18.5	25.3	30.4	5.1	7.5	9.3	10.6	12.3
30	8.8	14.9	20.4	25.7	30.9	5.0	6.5	8.2	10.2	12.1
40	9.4	15.3	20.5	26.1	31.4	4.4	5.9	8.1	10.0	11.7
50	10.4	15.4	20.9	26.3	31.5	3.9	5.8	8.0	9.6	11.3
60	10.4	15.6	21.7	26.4	31.5	3.7	5.8	7.7	9.3	10.9

median value) received power, corresponding to a probability of 99%,

$$D_{F1\%} = F_P^{-1}(0.5) - F_P^{-1}(0.01) \qquad (25)$$

B. DELAY SPREAD AND COHERENCE BANDWIDTH

Simulations were done for $R = 4, 6, 8, 10$ and 12 m, with a carrier frequency of 2.45 GHz, 5 000 (Tx, Rx) positions randomly distributed inside the circle being evaluated for each value of R. The delay spread was evaluated over all locations for each value of R, Figure 6.

The average, $\overline{\sigma_\tau}$, and the standard deviation, σ_{σ_τ}, of delay spread for different values of B was calculat, Table 2.

As expected, $\overline{\sigma_\tau}$ and σ_{σ_τ}, increase with R. For a given R, $\overline{\sigma_\tau}$ increases for increasing B, being almost constant for $B\tau_R$ above 0.63 as previously explained (corresponding to B_{C2nd}), which corresponds to $B = 47.3, 31.5, 23.6, 18.9$ and 15.6 MHz for $R = 4, 6, 8, 10$ and 12 m, respectively. One can see that $\overline{\sigma_\tau}$ takes values in the order of up to a few tens of nanoseconds, which can be considered to be acceptable; σ_{σ_τ} reaches a maximum around 16 ns, which is quite good.

The corresponding coherence bandwidth is presented in Figure 7. For B lower than the B_{D2nd}, B_c tends to infinity, hence, not being presented in the figure, which corresponds to a situation in which the channel behaves as a narrowband one. The inverse behavior of $\overline{\sigma_\tau}$ to $\bar{B}_c$ can be observed, being noticeable the constant behavior of $\bar{B}_c$ for B above B_{C2nd}. The range of values for $\bar{B}_c$ is around a few MHz (for a carrier frequency of 2.45 GHz) and does not change much for each R (roughly, up to 50% higher compared to the saturation value).
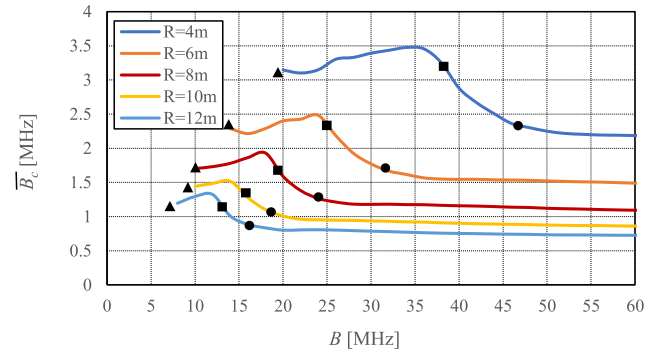

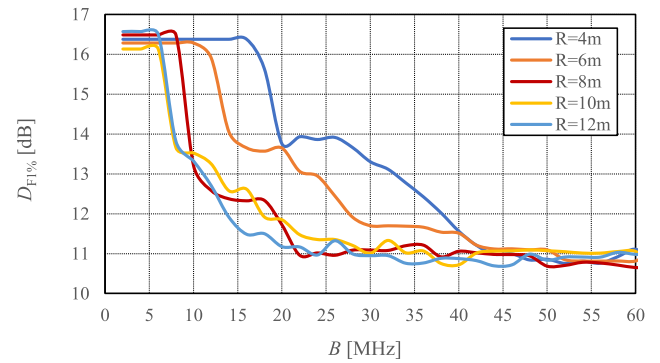**FIGURE 7.** Average coherence bandwidth vs. B for various R.

FIGURE 8. Fading depth for 99% probability vs. B for various R.

C. SHORT-TERM FADING DEPTH

In a proper system deployment design, one needs to account for the fading margins, namely the short-term ones, which depends on system bandwidth. In what follows, one analyses the fading depth for different system bandwidths, allowing to properly estimate the short-term fading margins that should be considered for a proper link budget evaluation. It should be remembered that the narrow- or wideband nature of a given system depends not only on its bandwidth but also on the coherence bandwidth of the propagation channel, i.e., on the environment properties; this implies that any given system can behave as narrow- or wideband, depending on the working environment being considered.

The fading depth, $D_{F1\%}$, is represented in Figure 8 as a function of system bandwidth, where one can observe that it is essentially composed of three main stages, depending on the value of B, up to 60 MHz.

The three stages are as follows: 1) as B increases, $D_{F1\%}$, is almost constant until a specific value of B is reached, after which it decreases; 2) then, $D_{F1\%}$, decreases rapidly until B reaches another specific value, beyond which it is almost constant; 3) for B higher than a given value, $D_{F1\%}$ is almost constant. These notable points are related to the breakpoints previous established, as shown Figure 9 for $R = 8$ m: the first almost constant behavior occurs up to B_{D2nd}, then the decrease occurs up to B_{C2nd}, beyond which it is almost
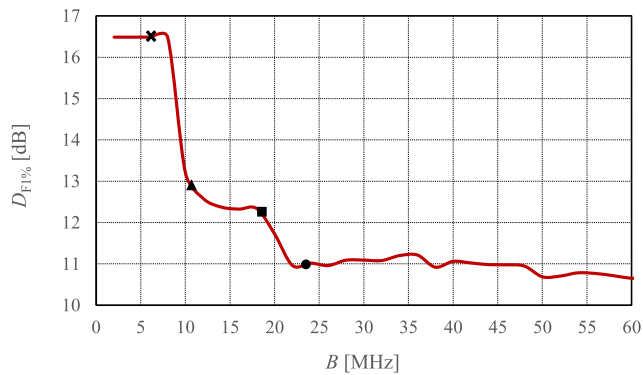
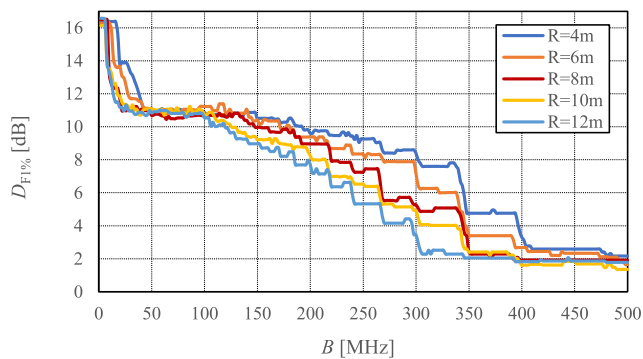**FIGURE 9.** Fading depth for R = 8m vs. B.

FIGURE 10. Fading depth vs. B for various R up to 500 MHz.

constant again. Regardless of R, the first constant level for $D_{F1\%}$ is slightly higher than 16 dB and the second one is around 11 dB, hence, the range being around 5 dB, which can be considered very good values for system design, i.e., the level of uncertainty is comparable with other usual cases in wireless communications.

The previous results were obtained for B up to 60 MHz, since it encompasses most system bandwidths of today's technologies working at the 2.4 GHz band. However, one should consider the possibility of having larger system bandwidths (which are already available for carriers in higher bands, namely mm waves).

In order to have an overview on the system behavior for larger bandwidths, Figure 10 presents $D_{F1\%}$ for B up to 500 MHz (a higher B means that the receiver is capable of discriminating in time more rays, hence, the contributions from higher order reflections).

One can observe that, for B larger than 100 MHz, $D_{F1\%}$ decreases with increasing values of B, the average decay rate being close to 3 dB per 100 MHz bandwidth, but after B reaching 400 MHz the behavior of $D_{F1\%}$ becomes almost constant again, with values about 2 dB. A similar behavior was already reported in [14] from measurements in the [3.1, 10.6] GHz band for indoor channels and in [15] for on-body wireless channels at 3.99 GHz.
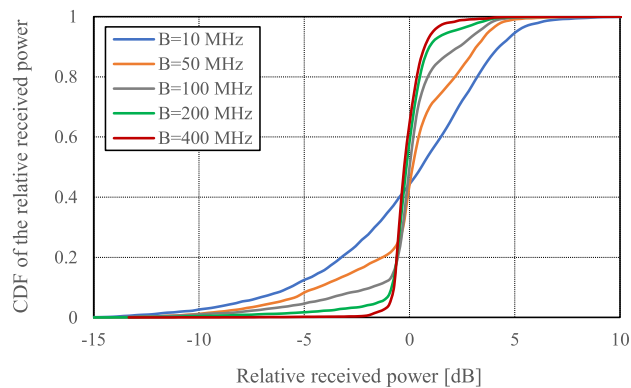

FIGURE 11. CDF of the relative received power for various B.

TABLE 3. Parameters of Linear Interpolation.

R [m]	$\Delta D_{F1\%}$ [dB/MHz]	D_0 [dB]	R^2	$\sqrt{\overline{\varepsilon^2}}$ [dB]
4	-0.023	14.2	0.88	0.75
6	-0.029	15.1	0.94	0.67
8	-0.033	15.1	0.96	0.56
10	-0.032	14.2	0.99	0.34
12	-0.033	13.8	0.97	0.51

It is also observed that the value of B for which $D_{F1\%}$ becomes almost constant tends to increase with the decrease of R, which is not surprising, since the value of B is related to the system ability to discriminate all arriving rays, namely the ones at close delays, i.e., the ones corresponding to situations where the Rx is close to the wall. For a given number of (Tx, Rx) positions randomly distributed inside the circle, the probability of the Rx being in the close proximity of the wall increases for decreasing values of R, hence, increasing the probability of CIRs with arriving waves at close delays. Therefore, increasing the value of B required to discriminate all arriving rays.

The staircase behavior of the fading depth for high bandwidths, with the height of stages increasing for increasing values of B, is due to the fact that for high bandwidths (above 100 MHz) a small variation of B can lead to a significant change in the value of fading depth, as seen in Figure 11, i.e., there is a saturation effect, which can be understood, since after a certain bandwidth the time interval for discrimination of rays becomes so small that is not differentiating among different reflections anymore.

In order to model the fading depth behavior for B ranging in [100, 400] MHz, one proposes a linear approximation,

$$D_{F1\%[dB]} = \Delta D_{F1\%[dB/MHz]} B_{[MHz]} + D_{0[dB]} \quad (26)$$

the values of $\Delta D_{F1\%}$ and D_0 being presented in Table 3.

The root mean square error, $\sqrt{\overline{\varepsilon^2}}$, varies in [0.34, 0.75] dB and the coefficient of determination, R^2 (one is using this usual notation for this coefficient, but it is not at all related to the radius R), takes values in [0.88, 0.99], which show that

TABLE 4. Average values and standard deviation of $D_{F1\%}$.

Stage	SBLow	SBMed	SBHig
$\overline{D_{F1\%}}$ [dB]	16.4	13.3	11.0
$\sigma_{D_{F1\%}}$ [dB]	0.1	1.5	0.3

the approximation is very good [16]. The values of $\Delta D_{F1\%}$ correspond to an average decrease of fading depth of 2.3 to 3.3 dB per 100 MHz bandwidth, hence, the 3 dB decay mentioned above.

IV. APPLICATION IN RADIO NETWORK PLANNING

The radio network planning process consists of evaluating possible required network configurations, including the location of base stations / access points, in order to achieve the required coverage with the desired capacity and quality of service. A complete dimensioning process includes link budget evaluation, for cell range and interference estimation, which encompasses the calculation of path loss in all its components, namely short-term fading margins [13]. These margins are usually obtained from Rice or Rayleigh Distributions (depending on the existence, or not, of an LoS component between the Tx and the Rx) for narrowband systems (system bandwidth smaller than the coherence bandwidth of the environment); however, when one considers wideband systems, the fading depth is smaller than the one obtained from the previous Distributions. Overestimating short-term fading margins, by considering these distributions, leads to shorter cells, or to higher transmitting powers, thus, higher interference, which is not desirable and can be overcome by taking more accurate fading margins. In this section one focus on the short-term fading margin evaluation as a function of B and R, i.e., of the characteristics of both the system and the environment.

The previous section shows that the fading depth is composed of three main stages in terms of system bandwidth, the transitions between these stages being associated with the system ability to discriminate arriving rays (i.e., multipath components) at the Rx: stage SBLow is associated to low values of B, where $D_{F1\%}$ is fairly constant; stage SBMed starts for values of B for which second order reflected rays start being discriminated by the receiver, B_{D2nd}, where $D_{F1\%}$ drops significantly; stage SBHig starts when more than 90% of second order reflected rays are discriminated, at B_{C2nd}, $D_{F1\%}$ being again fairly constant. Hence, one considers these breakpoints for evaluating average values of fading depth in each stage, Figure 12 showing the different stages and the borders between them, and Table 4 presenting the corresponding averages and standard deviations.

One can observe that the "platforms" for $D_{F1\%}$ occur at 16.4 and 11.0 dB, hence, with a difference lower than 6 dB (which is not very large), which were evaluated for $B < 60$ MHz. As previously mentioned, for 60 MHz $< B$ < 100 MHz the fading depth keeps almost constant, and for larger values the fading depth decreases being as low as 2 dB
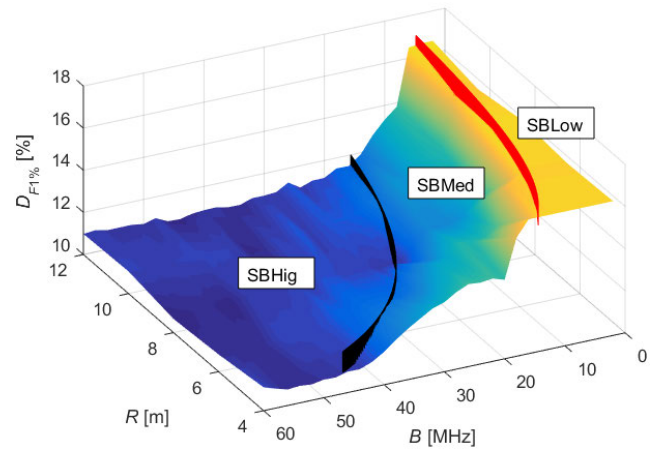

FIGURE 12. Fading Depth dependence on R and B.

TABLE 5. Fading Depth observed for different technologies.

Technology	Bandwidth [MHz]	$D_{F1\%}$ [dB]
LoRa	0.125/0.25/0.5	
ANT/ANT+		
IEEE 802.15.6	1	16.1 − 16.6
Bluetooth 5.2		
Bluetooth LE	2	
Zigbee		
IEEE 802.11b/g/n/ax	20	11.2 − 13.7
IEEE 802.11n/ax	40	10.7 − 11.6

for $B > 400$ MHz. It is also observed in Figure 12, in the SBMed stage, that $D_{F1\%}$ decreases with increasing B as well as increasing R. Basically, the higher the system bandwidth the lower the room size above which lower fading depths are observed.

As a conclusion, considering the current communication standards at the 2.4 GHz band suited for BAN applications purposes, one can recommend the fading margin that should be considered for planning purposes, as shown in Table 5.

These values take the system bandwidth into account, i.e., in general, systems with larger bandwidths should have smaller fading margins.

V. CONCLUSION

In this paper, the bandwidth dependent characteristics of the propagation channel for BANs in indoor circular metallic environments is studied. The main novelty of this work is the bandwidth dependent approach for the fading depth evaluation being proposed, allowing to evaluate appropriate short-term fading margins, in the aforementioned environments. Additionally, bandwidth dependent values of delay spread are also presented and discussed.

The originality of this work lies in the fact that several studies in the literature address channel characterization in

specific environments, but none address either the particular aspects of BANs or the specific problem of circular metallic structures, being considered here.

The proposed approach is based on a model that was assessed with measurements in a specific circular metallic environment, with extreme situations being analyzed analytically, which imposes limitations concerning its applicability to other kind of environments. Although other geometries cannot be analyzed with this model, the same approach can be taken for non-metallic environments.

Values originating the analysis come from measurements and simulations, with extreme cases on the location of transmitters and receiver being analyzed in an analytical approach, enabling a better understanding of the results and of the subsequent recommendations.

Globally, for system bandwidth up to 60 MHz the observed fading depths are comprised into three main stages, with the transitions between them being associated with the system ability to discriminate the arriving rays at the receiver. For increasing values of the system bandwidth, at the first stage, for low values of B, the fading depth is reasonably constant, then in the second stage (starting when second order reflected rays start being discriminated by the receiver), it decreases with a relatively high pace, and then in the third stage, for high values of B, which corresponds to more than 90% of second order reflected rays being discriminated, it reaches another constant platform. Average values of fading depth are 16.4 and 11.0 dB for the first and third stages. For B larger than 100 MHz, the fading depth decreases with increasing values of B, being as low as 2 dB for B larger than 400 MHz.

As a final system design recommendation, for network planning purposes, short-term fading margins ranging from 10.7 to 16.6 dB should be considered for current technologies suited for BAN applications at the 2.4 GHz band, depending on their system bandwidth.

REFERENCES

[1] H. Kdouh, C. Brousseau, G. Zaharia, G. Grunfelder, and G. E. Zein, "Measurements and path loss models for shipboard environments at 2.4 GHz," in *Proc. 41st Eur. Microw. Conf.*, Manchester, U.K., Oct. 2011, pp. 408–411.

[2] A. Mariscotti, M. Sassi, A. Qualizza, and M. Lenardon, "On the propagation of wireless signals on board ships," in *Proc. IEEE Instrum. Meas. Technol. Conf.*, Austin, TX, USA, May 2010, pp. 1418–1423.

[3] X. H. Mao, Y. H. Lee, and B. C. Ng, "Wideband channel characterization along a lift shaft on board a ship," in *Proc. IEEE Antennas Propag. Soc. Int. Symp.*, Toronto, ON, Canada, Jul. 2010, pp. 1–4.

[4] E. Balboni, J. Ford, R. Tingley, K. Toomey, and J. Vytal, "An empirical study of radio propagation aboard naval vessels," in *Proc. IEEE-APS Conf. Antennas Propag. Wireless Commun.*, Waltham, MA, USA, Nov. 2000, pp. 157–160.

[5] G. B. Tait and M. B. Slocum, "Electromagnetic environment characterization of below-deck spaces in ships," in *Proc. IEEE Int. Symp. Electromagn. Compat.*, Detroit, MI, USA, Aug. 2008, pp. 1–6.

[6] K. K. Cwalina, S. J. Ambroziak, P. Rajchowski, and L. M. Correia, "Radio channel measurements in 868 MHz off-body communications in a ferry environment," in *Proc. XXXII Gen. Assem. Sci. Symp. Int. Union Radio Sci. (URSI GASS)*, Montreal, QC, Canada, Aug. 2017, pp. 1–4.

[7] F. D. Cardoso, P. T. Kosz, M. M. Ferreira, S. J. Ambroziak, and L. M. Correia, "Fast fading characterization for body area networks in circular metallic indoor environments," *IEEE Access*, vol. 8, pp. 43817–43825, 2020.

[8] M. S. Derpich and R. Feick, "Second-order spectral statistics for the power gain of wideband wireless channels," *IEEE Trans. Veh. Technol.*, vol. 63, no. 3, pp. 1013–1031, Mar. 2014.

[9] G. D. L. Roche and C.-C. Chong, "Bandwidth dependency channel model: On the impact to carrier aggregated systems," in *Proc. IEEE Wireless Commun. Netw. Conf.*, Cancun, Mexico, Mar. 2011, pp. 1846–1851.

[10] G. Gaertner and E. O. Nuallain, "Characterizing wideband signal envelope fading in urban microcells using the Rice and Nakagami distributions," *IEEE Trans. Veh. Technol.*, vol. 56, no. 6, pp. 3621–3630, Nov. 2007.

[11] F. D. Cardoso and L. M. Correia, "A time-domain based approach for short-term fading depth evaluation in wideband mobile communication systems," *Wireless Pers. Commun.*, vol. 35, no. 4, pp. 365–381, Dec. 2005.

[12] F. D. Cardoso and L. M. Correia, "Fading depth dependence on system bandwidth in mobile communications—An analytical approximation," *IEEE Trans. Veh. Technol.*, vol. 52, no. 3, pp. 587–594, May 2003.

[13] D. Parsons, *The Mobile Radio Propagation Channel*. London, U.K.: Pentech Press, 1992.

[14] W. Q. Malik, B. Allen, and D. J. Edwards, "Impact of bandwidth on small-scale fade depth," in *Proc. IEEE Global Telecommun. Conf.*, Washington, DC, USA, Nov. 2007, pp. 3837–3841.

[15] V. Sipal, D. Gaetano, P. McEvoy, and M. J. Ammann, "Bandwidth scaling of fading properties of on-body wireless channel in body area networks," in *Proc. 10th Int. Conf. Commun. (COMM)*, Bucharest, Romania, May 2014, pp. 1–4.

[16] H. Cramér, *Mathematical Methods of Statistics*. Princeton, NJ, USA: Princeton Univ. Press, 1999.

MANUEL M. FERREIRA (Member, IEEE) received the Licenciado degree in electronics and telecommunications from the University of Aveiro, and the M.Sc. degree in electrical and computer engineering from the IST, Technical University of Lisbon. Since 1995, he has been with the Department of Electrical Engineering, ESTSetúbal, Polytechnic Institute of Setúbal, Portugal, where he is currently a Professor in telecommunications and electronics. He was involved in European projects and networks of excellence COST CA20120, COST CA15104, NEWCOM, and ICT/LEXNET. His research interests include wireless/mobile channel characterization and wireless sensor and body area networks.

FILIPE D. CARDOSO (Member, IEEE) received the Licenciado, M.Sc., and Ph.D. degrees in electrical and computer engineering from the IST, Technical University of Lisbon. Since 1994, he has been with the Department of Electrical Engineering, ESTSetúbal, Polytechnic Institute of Setúbal, Portugal, where he is currently a tenured Professor in telecommunications and the Head of the Electronics and Telecommunications Area. He is also a Researcher with INESC-ID, Lisbon. He was or is involved in European projects and networks of excellence COST 273, COST IC1004, COST CA15104, COST CA20120, IST/FLOWS, ICT/4WARD, ICT/EARTH, ICT/LEXNET, NEWCOM, and NEWCOM++. He was the Task Leader of Energy Efficiency in Transmission Techniques (EARTH) and Dissemination and Standardization (LEXNET) workgroups. He has authored papers in national and international conferences and journals, for which he has also served as a reviewer and a board member. He was the Secretary of the IEEE ComSoc Portuguese Chapter. His research interests include wireless/mobile channel characterization and modeling, body area networks, and mobile broadband systems.

SŁAWOMIR J. AMBROZIAK (Senior Member, IEEE) was born in Poland, in 1982. He received the M.Sc., Ph.D., and D.Sc. degrees in radio communication from the Gdańsk University of Technology (Gdańsk Tech), Poland, in 2008, 2013, and 2020, respectively. Since 2008, he has been with the Department of Radio Communication Systems and Networks, Gdańsk Tech, as a Research Assistant, from 2008 to 2013, as an Assistant Professor, from 2013 to 2020, and as an Associate Professor, since 2020. He is the author or coauthor of many publications, including book, book chapters, articles, reports, and papers presented during international and domestic conferences. He has participated and still participates in several projects related to special application of wireless techniques and three COST Actions (IC1004, CA15104, and CA20120). His currently research interest includes radio channel modeling in body area networks. He was a recipient of the Young Scientists Awards of URSI, in 2016 and 2011, and many domestic awards. He is a Senior Member of URSI and a member of the Gdańsk Scientific Society. He is also a member of the European Association on Antennas and Propagation (EurAAP) Delegate Assembly, a Management Committee Member of the COST CA20120 Action, the Vice-Chair of Commission-F of the Polish National Committee of URSI, and an Expert in the Electronics and Telecommunications Committee of the Polish Academy of Sciences. In previous years, he was a member of the Board of the Working Group on Propagation of EurAAP, and a Management Committee Substitute Member of the COST CA15104 Action.

LUIS M. CORREIA (Senior Member, IEEE) was born in Portugal, in 1958. He received the Ph.D. degree in electrical and computer engineering from the IST, University of Lisbon, in 1991. He is currently a Professor in telecommunications with the IST, University of Lisbon, with his work focused on wireless and mobile communications, with the research activities developed in the INESC-ID Institute. He is currently an Honorary Professor with the Gdańsk University of Technology, Poland. He has acted as a Consultant for the Portuguese telecommunications operators and regulator, besides other public and private entities, and has been in the Board of Directors of a telecommunications company. He has participated in 32 projects within European frameworks, having coordinated six and taken leadership responsibilities at various levels in many others, besides national ones. He has supervised over 230 M.Sc./Ph.D. students, having edited six books, contribute to European strategic documents, and authored over 500 papers in international and national journals and conferences, for which served also as a reviewer, an editor, and a board member. Internationally, he was part of 40 Ph.D. juries, and 78 research projects and institutions evaluation committees for funding agencies in 12 countries, and the European Commission and COST. He was a recipient of the 2021 EurAAP Propagation Award for leadership in the field of propagation for wireless and mobile communications. He has been the Chairperson of Conference, Technical Program Committee, and Steering Committee of 25 major conferences, besides other several duties. He was a National Delegate to the COST Domain Committee on ICT. He has launched and served as the Chairman of the IEEE Communications Society Portugal Chapter, besides being involved in several other duties in this society at the global level.

. . .